Decrease of the spatial variability and local dimension of the Euro-Atlantic eddy-driven jet stream with global warming

Robin Noyelle, Vivien Guette, Akim Viennet, Bénédicte Colnet, Davide Faranda, Andreia Hisi, Pascal Yiou

Decrease of the dynamical and spatial variability of the Euro-Atlantic eddy-driven jet stream with global warming

Robin Noyelle[1*†], Vivien Guette[1†], Akim Viennet[1†] and Davide Faranda[1,2,3]

[1]Laboratoire des Sciences du Climat et de l'Environnement, LSCE/IPSL, CEA-CNRS-UVSQ, Université Paris-Saclay, Gif-sur-Yvette, 91191, France.
[2]London Mathematical Laboratory, 8 Margravine Gardens London, W6 8RH, London, United Kingdom.
[3]LMD/IPSL, Ecole Normale Superieure, PSL research University, Paris, France.

*Corresponding author(s). E-mail(s): robin.noyelle@lsce.ipsl.fr;
Contributing authors: vivien.guette@lsce.ipsl.fr;
akim.viennet@lsce.ipsl.fr; davide.faranda@lsce.ipsl.fr;
†These authors contributed equally to this work.

Abstract

The atmospheric eddy-driven jet stream is one of the main features of the mid-latitude circulation. Although mostly zonal in climatological mean, the jet stream meanders at meteorological time scales. The jet and its variability have been under great scrutiny in the past years for their role in the triggering of extreme events (e.g. heat or cold waves) in mid-latitudes regions. Because of the large variability of the jet, the impact of climate change remains elusive. Here we study the eddy-driven jet stream over the Euro-Atlantic sector and assess its dynamical properties in ERA5 and ERA20C reanalysis data set using indicators from dynamical system theory. We then use a causal framework to disentangle the impact of global warming from the impact of natural variability of the climate system on the jet. We find that over the period 1900-2010, global warming decreased the spatial and dynamical variability of the jet. This decrease in variability is connected to an increase in jet

persistence and speed. We additionally observe a poleward shift of the jet. Our results suggest a zonalisation of the jet under global warming.

Keywords: jet stream, global warming, causal analysis, inter-decadal variability

1 Introduction

Jet streams are narrow, fast-flowing westerly air currents in the troposphere. They are a major feature of the large-scale atmospheric circulation and modulate the frequency, severity and persistence of weather events across the extratropics (Charney, 1947; Holton, 1973; Hurrell and Deser, 2010). Two types of atmospheric jets can be identified: thermally driven subtropical jets associated with the eastward deflection of the upper branch of the Hadley cell (Held and Hou, 1980), and eddy-driven jets caused by the transfer of energy from baroclinic eddies to the mean flow at the polar front (Held, 1975; Rhines, 1975). Real jets may arise from a combination of these mechanisms and thermally and eddy-driven jets are actually two limits in a continuous spectrum (Lee and Kim, 2003; Spensberger and Spengler, 2020; Messori et al, 2021).

Even though the climatological eddy-driven jet is mostly zonal flowing to the east, on a daily basis it can present large meanders. In these cases, the local flow becomes predominantly meridional or can even split or break. Those meanders have a typical spatial and temporal variability of a few thousand kilometers and of 10 days (Röthlisberger et al, 2016). The meanders allow air masses coming from the south or the north to persist around mid-latitude regions, potentially triggering temperature or precipitation extremes (Kautz et al, 2022). For its role in the triggering of extreme events in mid-latitude regions, the eddy-driven jet has been under great scrutiny in the past years.

The variability of the eddy-driven jet stream is an example of the large spontaneous variability of the climate system. The inter-decadal jet variability is important, with decades of strong and steady jet being interspersed with decades of a weak and more variable jet (Woollings et al, 2018; Simpson et al, 2019; Osman et al, 2021). Therefore, identifying the impact of global warming on the jet has remained elusive and controversial (Barnes and Screen, 2015). Even though there is a broad agreement on the poleward shift of the eddy-driven jet with global warming (Pena-Ortiz et al, 2013; Woollings et al, 2014; Lee et al, 2021), the impact of global warming on the other characteristics of the jet are still unclear (Stendel et al, 2021). Indeed, the jet has been caught in the 'tug-of-war' (Held, 1993) between two competing phenomena: the Artic amplification (AA) and the tropical upper-tropospheric warming.

As the Artic is warming more rapidly than the rest of the world (Cohen et al, 2018) – reducing the Arctic-to-mid-latitude geopotential gradient – it has been argued that this could lead to changes in the configuration of the jet stream (Francis and Vavrus, 2015). The reduced equator-to-pole temperature

gradient could weaken the predominant westerly winds, which, in turn, could cause larger-amplitude waves in the midlatitude circulation. However, global warming also leads to tropical upper-tropospheric warming, which would in contrary act to increase the equator to pole gradient of temperature, reinforcing the jet (Stendel et al, 2021). Another mechanism could increase the waviness of the jet: the increased land-sea gradients under global warming, as supported by the recent theoretical work of Moon et al (2022).

Changes in the latitudinal or longitudinal temperature gradients are however not the only mechanisms through which the dynamics of the jet could have changed during the 20th century. Antropogenic aerosols emissions and internal variability of the climate system are two other competing factors. Several studies have demonstrated the role of antropogenic aerosols in changing the dynamics of the North Atlantic atmosphere (e.g. Pausata et al (2015); Diao and Xu (2022); Murakami (2022)) through anomalous heating or cooling in the mid-latitudes. Low frequency variability of the ocean is another confounding phenomenon. The Atlantic Multidecadal Oscillation (AMO), a 60–80 year basinwide quasi-oscillation in North Atlantic sea surface temperatures (Kerr, 2000), can be invoked to explain the intedecadal changes in the dynamics of the jet. The variations in the coupled El-Nino-Southern Oscillation (ENSO) and Pacific Decadal Oscillation (PDO) could also influence the variability of the jet through the generation of Rossby wave trains (Ding et al, 2017; Mezzina et al, 2020).

Studies on reanalysis data have shown conflicting results on the evolution of jets under global warming with some of them concluding to a weakening of the North Atlantic jet (Francis and Vavrus, 2015; Coumou et al, 2015; Harvey et al, 2020), while others concluded to a stronger jet under global warming (Iqbal et al, 2018; Tenenbaum et al, 2022; Hallam et al, 2022). Some studies have also targeted directly the measurement of the "waviness" of the midlatitude circulation, with various metrics (Cattiaux et al, 2016; Peings et al, 2018; Blackport and Screen, 2020). A common theme of those studies is that the natural variability of the jet stream may be a sufficient explanation to the recent observed increases of its waviness (Osman et al, 2021; Blackport and Screen, 2020). Therefore, the recent observed covariability between waviness and temperature gradients on interannual to decadal time scales may not represent a forced response.

Here, we address the question of quantifying the changes in the characteristics of the Euro-Atlantic eddy-driven jet stream due solely to global warming over the 20th century.

Several approaches have been developed to detect the eddy-driven jet stream position from wind and pressure maps, each with advantages but also limitations. Some algorithms were developed to capture the 3D (Limbach et al, 2012) or 2D structure (Molnos et al, 2017; Spensberger et al, 2017) of the jet. A large part of the literature investigating the jet variability however reduces the jet to a single point characterized by a latitude, the so-called Jet Latitude Index (JLI), and a wind speed by finding the point where the zonally averaged

low-level zonal wind is maximum (Woollings et al, 2010). This method provides useful insights and is very handful to make time-series statistics using only two indexes, nonetheless it misses key geometric features of the jet such as the omega-shaped pattern associated with blocking events. Here we adopt a more geometric view by considering the latitudinal position of the jet at each longitude (Faranda et al, 2019b).

We analyze this representation of the jet with recently developed indicators (Lucarini et al, 2016; Faranda et al, 2017; Messori et al, 2021) based on dynamical systems theory. We expand the results of Faranda et al (2019a) and Rodrigues et al (2018) who have shown the interest of using time series of these indicators to detect changes in the large scale circulation. Here we target specifically the eddy-driven jet. We finally employ a causal framework (Kretschmer et al, 2021) based on the existing climate knowledge to control for the influence of confounding factors – internal variability and anthropogenic aerosols emissions – and quantify the sole effect of global warming on various indicators of the jet variability.

This paper is organized as follows: in Section 2, we introduce the data used and the methods developed to detect the jet stream position and quantify its variability. In Section 3, we assess the ability of our indicators to characterize the jet variability by investigating how they are related to other jet characteristics. We also show the relevance of targeting specifically the jet as an atmospheric feature rather than studying sea-level pressure or geopotential maps. In Section 4, we investigate the interdecadal variability of the eddy-driven jet over the 20th century and relate it to classical indices of natural variability. Finally, the discussion of the results and the conclusions drawn from our analysis are presented in section 5.

2 Data and methods

2.1 Data

The analyses proposed here are based on the ERA5 reanalysis data of the European Centre for Medium range Weather Forecasts (Hersbach et al, 2020). We use daily averaged fields with a 0.25° horizontal resolution over the 1950–2021 period for the Euro-Atlantic region from 22.5°N to 70°N in latitude and from 80°W to 50°E in longitude. For disentangling the role of natural and forced response on the low-frequency evolution of the jet variability, we use the ERA20C reanalysis dataset, which is the 20th century reanalysis of the ECMWF (Poli et al, 2016), over the 1900–2010 period with the same spatial extension. This dataset has a resolution of 1.125°. For both data sets, the variables considered are the daily-averaged geopotential height at 500hPa (Z500), sea-level pressure (SLP) and horizontal wind speed between 850 and 700hPa.

For quantifying the link between the variability of the jet position, classical indices of natural variability and global warming, we use monthly indices downloaded from the Climate Explorer web tool. For the AMO, we use the

AMO index of the Met Office Hadley Centre/Climatic Research Unit (van Oldenborgh et al, 2009). This index corresponds to the average of monthly Sea Surface Temperature (SST) anomalies with respect to the ensemble mean of the reanalysis over the North Atlantic. For the PDO, we use the PDO index of the Hadley Center based on an EOF decomposition of Pacific SSTs. For the ENSO we take the Nino 3.4 index, which is the area averaged SST from 5S-5N and 170-120W (Van Oldenborgh et al, 2021). For quantifying global warming, we use the monthly global mean Earth surface temperature anomalies (relative to the 1961–1990 period) provided by the Hadley Centre (HadCRUT5 data set, Morice et al (2021)). For the AMO, PDO and ENSO indices a linear trend has been removed to account for the global warming signal.

We further consider the impact of aerosols forcing. We use the ambient aerosol absorption optical thickness at 550nm provided at a monthly time scale by the IPSL model (Dufresne et al, 2013) under the CMIP5 historical configuration for the 1900-2000 period and under the RCP4.5 scenario for the period 2000-2020. The optical thickness is provided at each grid point and we average the field over the same Euro-Atlantic sector as for ERA5 and ERA20C. The ERA5 and ERA20C reanalyses both use the CMIP5 forcing files for aerosols concentration (Poli et al, 2016; Hersbach et al, 2020), which consists of monthly 10 year-averaged files.

2.2 Detecting the jet position

For detecting the jet position, we first average over 850–700hPa pressure levels the horizontal wind speed. Contrary to Woollings et al (2010), we investigate the variability of the jet not only over the North Atlantic ocean. In order to avoid boundary layer effects over continental Europe we prefer to begin the averaging process at a higher pressure level: 850hPa rather than 925hPa. We then apply a 10 days low-pass Lanczos filter with a window of 61 days to remove the influence of transient eddies (Duchon, 1979). At this point we do not apply a zonal mean but take a two-step approach close to the procedure used by Faranda et al (2019b). The first step consists in finding, for each longitude, the latitude at which the wind horizontal kinetic energy $E = \frac{1}{2}\vec{u}_H^2$ is maximum. The second step is to apply a 25° of longitudes rolling median to the previous positions. This rolling median is applied to avoid a nonphysical detection of breaks in the jet. With a 0.25° horizontal resolution for ERA5 and considering the low-level jet, the algorithm sometimes detects high-wind speeds in the lee of mountains. 25° of longitudes approximately corresponds to 2000km at 45°N, which is also the typical size of mid-latitude baroclinic disturbances (Hoskins and James, 2014) so that we consider that this rolling median has a physical basis. An example of the jet position found with this method is given in figure 1.

Our approach considers the jet position as a vector of positions indexed by longitudes. However, vectors are not easy to study as time series and we need to reduce the dimension to summarize these objects to single values. The following sections present the indicators we used.

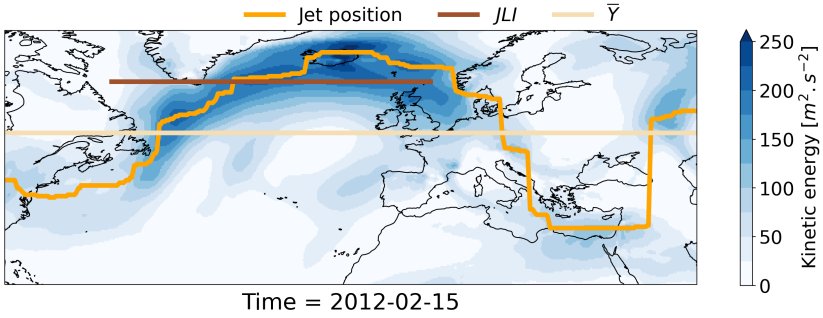

Fig. 1 Snapshot of the horizontal wind kinetic energy and jet position for one example day. Wind horizontal kinetic energy $E = \frac{1}{2}\vec{u}_H^2$ (colors) and jet position found by the algorithm (orange line). The yellow and brown lines represent respectively the jet latitude index JLI and the mean position of the jet $\bar{Y}$ found with our method.

2.3 Dynamical indicators

In physics, dynamical systems can be defined as objects whose states vary with time. In atmospheric physics in particular, fields such as sea-level pressure, temperature or precipitation can be considered as observables of a dynamical system, namely the atmospheric flow (Lucarini et al, 2016; Faranda et al, 2017). In our case, the observable we are studying is the jet position at each longitude, going through different daily states, noted ζ. A state of our system can be described as a vector of dimension lon where lon represents the number of grid points along the longitudinal axis. The y^{th} position in this vector contains the latitudinal value of the jet position for the y^{th} longitude. The ensemble of states of the jet at all time approximate the dynamics of the atmospheric flow and should retain some of the properties of the full, high dimensional, attractor of mod-latitude atmospheric motions.

We define two indicators to characterize our dynamical system: the local dimension d and the local persistence θ^{-1} which both characterise instantaneous state of the system in the phase space (Lucarini et al, 2016; Faranda et al, 2017). Both of these indicators are computed using the fact that the probability for a recurrence of a system configuration (a state) can be linked to the generalized Pareto distribution (Pickands, 1975). To compute this probability from data, we compute the series of distances $\text{dist}(x(t), \zeta)$ between a state of the system ζ and all other points $x(t)$ on the trajectory of the system. This time series of distances is then transformed into: $g(t) = -log(dist(x(t), \zeta))$ so that being close to state ζ is equivalent to exceeding a threshold $s(q)$ where q is a percentile of the series $g(t)$. We use the 98% percentile of all values of $g(t)$, which ensures to have enough data while keeping only the extremes. For the calculation of the distances between states, we use the Euclidian distance. It can be shown that the probability distribution of $g(t)$ when it exceeds $s(q)$ converges to a Pareto distribution (Lucarini et al, 2016) with scale parameter σ, and a shape parameter $\xi = 0$.

The local dimension d is practically estimated as the inverse of the scale parameter of the generalized Pareto distribution fitted on the data which satisfies $g(t) > s(q)$. d is a proxy for the system's active number of degrees of freedom when reaching a region of phase space. Thus, even when considering a system with a large number — possibly infinite — of dimensions, d provides the local number of dimensions that the system can be summarized to. Therefore a state 1 with a local dimension d_1 greater than the local dimension d_2 of another state 2 means that the behavior of the system around state 1 has more dimensions on which to evolve and is therefore less predictable than around state 2 (Messori et al, 2017; Hochman et al, 2019). Additionally, Pons et al (2020) showed that d can be used as a measure of co-dependance: a high degree of synchronization between the variables defining the system is associated with a low value of d.

The second dynamical system indicator we use is the persistence θ^{-1} of a given state ζ, which is equivalent to the mean residence time of the trajectories when they enter the neighborhood of ζ. This metric corresponds to the inverse of a well defined statistical quantity introduced in extreme value statistics, namely the extremal index θ. The latter is here estimated using the Süveges (2007) estimator on the time series $g(t)$. Note that in the framework of dynamical systems, we find $\theta = 0$ at stable fixed points of the dynamics (the trajectory resides an infinite amount of time in the neighborhood of this state), with an infinite number of infinitely time resolved trajectories. Conversely, $\theta = 1$ is found at non persistent states of the dynamics (see Moloney et al (2019) for more details). In general, for time-continuous systems sampled at a given resolution dt, $\theta^{-1} > 1$. For daily sea-level pressure fields over the North Atlantic, Faranda et al (2017) found θ^{-1} values varying between 2 and 3 days. One may note that these values depend on the size and the timestep of the data set used, and on the chosen percentile q. Therefore the local persistence θ^{-1} is to be used to compare different states within the same data set.

2.4 Other variability indicators

To the local dimension d and persistence θ^{-1} indicators we add three other indicators of the jet stream state for analysing its variability. For each day we compute :

- the jet mean position $\bar{Y}$, defined as the zonal average of the jet positions found with the detection algorithm. As illustrated in Fig. 1 one should note that this indicator is not equivalent to the JLI for two reasons: (i) our indicator is computed on the full Euro-Atlantic sector and not only over the North Atlantic and (ii) the mean position is computed without applying a zonal average to zonal wind speed;
- the jet mean speed $\bar{U}$, defined as the zonal average of the norm of the horizontal wind vector $\vec{u}_J$ at the jet position: $\bar{U} = \frac{1}{lon} \sum_{lon} \sqrt{u_J^2 + v_J^2}$. For each longitude, the horizontal wind vector $\vec{u}_J$ is computed as the mean

of horizontal wind vectors within a 2.5° latitudinal extent around the jet position. Again, this indicator is not equivalent to the zonal jet speed as defined in Woollings et al (2010);

- the jet waviness W, defined as the longitudinal standard deviation of the jet position. Before computing this parameter, we remove a linear spatial trend to the jet position as the jet has a tendency to present a northward tilt over the North Atlantic. This indicator is always positive and indicates a jet without (with) meanders when taking low (high) values.

In addition to our indicator $\bar{Y}$ and $\bar{U}$, we also use the more classical jet latitude index JLI and zonally-averaged zonal wind speed U_{JLI}. There is no universally accepted metric to measure the "waviness" of mid-latitude circulation and therefore several measures have been used in the literature (Blackport and Screen, 2020). Our measure of waviness W is straightforward to compute, intuitive and gives easily interpretable results. We note that our approach is close to the sinuosity metric proposed by Cattiaux et al (2016).

3 Diagnosing the jet variability

Faranda et al (2017) made the case for the use of dynamical indicators to investigate the weather variability over the Euro-Atlantic sector with the tools presented in 2.3 using SLP as a state vector. Here we specifically target the jet position (Faranda et al, 2019b; Messori et al, 2021). Figure 2 presents the cross distribution of d and θ^{-1} computed on SLP, Z500 and jet positions reanalysis data over the Euro-Atlantic sector. The dynamical indicators for SLP and Z500 are strongly correlated (Pearson correlation coefficient $r = 0.45$ for d and $r = 0.71$ for θ^{-1}), which was expected in so far as those fields carry similar information about the synoptic meteorological state of the atmosphere. Conversely, almost no correlation is observed between the dynamical indicators computed on the jet position and the one computed on the SLP or the Z500. As previously, this illustrates that the variability of the jet position cannot be reduced to the variability of the SLP and Z500 fields (Dorrington and Strommen, 2020).

The absolute values of the indicators can be compared from one data set to another in so far as they have a similar sampling frequency. The mean local dimension found for the ERA5 data set is 7.6. With a different spatial resolution (0.25° vs 1.125°), we find a mean value of 7.5 for the ERA20C data set. These values must be compared with the values of 11.4 and 13.5 for the mean local dimension of the Z500 and SLP fields on the ERA5 data set. For the persistence, we find values evolving in the same range for the three variables (between 2 and 3 days).

Figure 3 panel (c) displays the cross distribution of points for the dynamical indicators d and θ^{-1} computed on the jet position vectors. The marginal distributions are shown in Fig. 3 panel (a) and (d). The points are colored with respect to which tercile of the distribution of the waviness indicator W they belong to (Fig. 3 panel (b)). The less wavy jets are associated with high

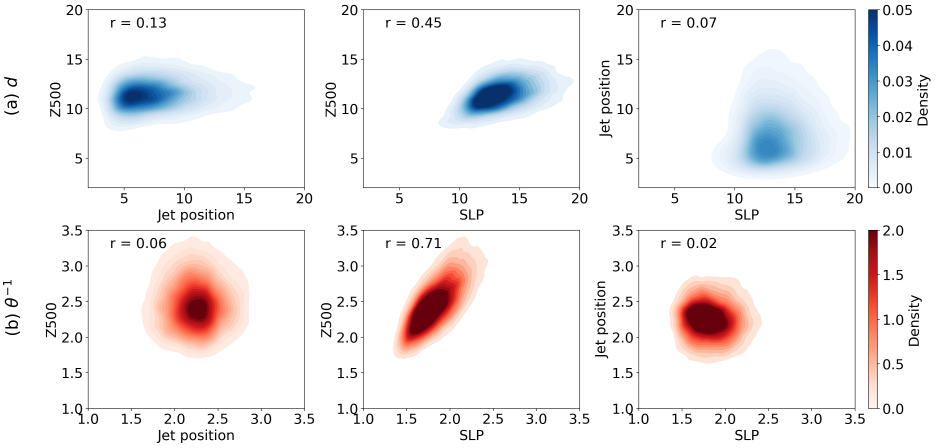

Fig. 2 Cross distributions of dynamical indicators for Z500, SLP and jet positions (ERA5). (a) Cross distributions of the local dimension d between the Z500 field and jet position, the Z500 field and the SLP field, and jet position and the SLP field. (b) Cross distributions of the local persistence θ^{-1} between the Z500 field and jet position, the Z500 field and the SLP field, and jet position and the SLP field. For computational reasons, the dynamical indicators on the Z500 and the SLP fields have been computed with a spatial resolution of 0.5° instead of 0.25°.

values of θ^{-1} and low values of d while the most wavy jets are found to have lower values of θ^{-1} and higher values of d. These results are consistent with what Messori et al (2021) found using an idealised quasi-geostrophic model and computing indicators on the wind field. Figure 9 and 10 in annex present the same analysis for the $\bar{U}$ and $\bar{Y}$ indicators. Contrary to Fig. 3, the d and θ^{-1} indicator have difficulties discriminating the jet dynamical behavior when using the mean speed and mean position, which suggests that $\bar{U}$ and $\bar{Y}$ are not the most relevant indicators to capture the dynamical properties of the jet.

As in Faranda et al (2017) and Messori et al (2017), to better understand what kind of dynamical information the indicators reveal, we analyze the extreme cases of the d and θ^{-1} indicators. We take the composite maps over the days belonging to the top 2% in term of one of the indicator and for which the other one is not extreme (in the sense that it does not belong to the top 2% neither to the bottom 2% quantiles). We define four situations: low local dimension (N=377 days of observations), high local dimension (N=458 days of observations), low local persistence (N=457 days of observations) and high local persistence (N=357 days of observations), which are presented in Figure 4.

In the high local dimension case, the synoptic meteorological situation shows no clear pattern, and the density of the jet position is widespread. This behavior is consistent with the concept of local dimension: for points with a very high local dimension, the system has many degrees of freedom and can correspond to many dynamical situations. In the low local dimension case, the density of the jet stream position shows a bi-modality over the eastern

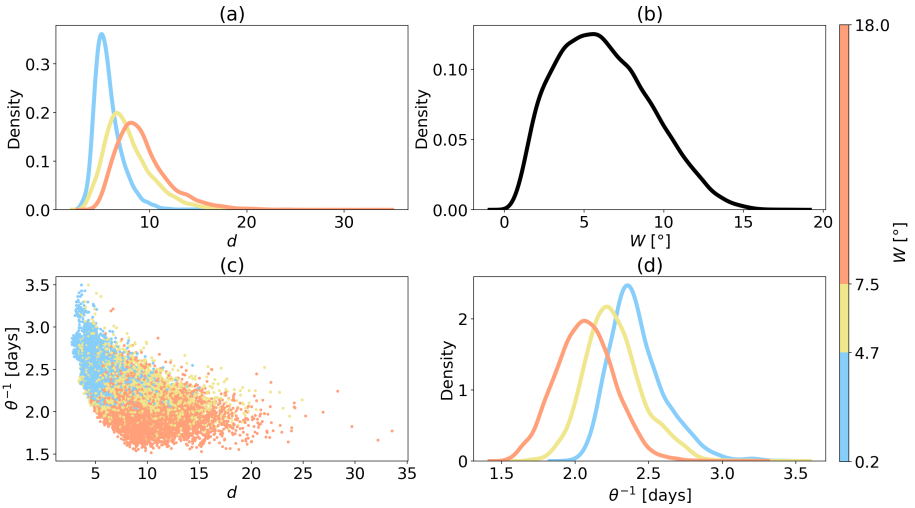

Fig. 3 Link between the dynamical indicators and the jet waviness (ERA5). (a) Distribution of local dimension d for the three terciles of the waviness W. (b) Distribution of W. (c) Cross distribution of d and θ^{-1} colored by the tercile of the W indicator. (d) Distribution of local persistence θ^{-1} for the three terciles of the waviness W.

part of the American continent and a tri-modality over the European continent, leading to five distinct clusters of trajectories. The two main modes represented by black dashed lines count for approximately 60% of all the trajectories. The synoptic situation displays a large anticyclone over North-Western Europe reminiscent of the NAO+ weather regime but is associated with several possible patterns of the jet.

In the low local persistence case, the anomalies of SLP show a pattern, close to the Scandinavian Blocking situation. The averaged jet pattern is peculiar but nonetheless well defined – in so far as there is a low dispersion of the jet position density – and has a pronounced dip over the Mediterranean Sea in its main mode (80% of the trajectories). This very wavy situation of the jet is reminiscent of recent synoptic situation corresponding to temperature extremes over Western Europe (e.g. Mitchell et al (2019)). Finally, the high local persistence case is reminiscent of the NAO- situations with a positive SLP anomaly over Greenland and a negative slp anomlay over the Azores (Michelangeli et al, 1995).

We now turn to using these indicators to study the recent past evolution of the Euro-Atlantic eddy-driven jet stream and its relation to usual modes of variability of the climate. In the following, we mainly display results based on the ERA20C data set because it spans a longer time period. The corresponding results for the ERA5 data set are presented in annex.

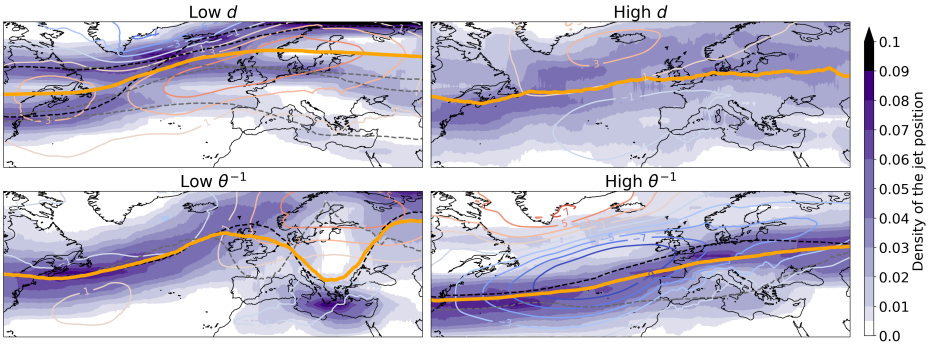

Fig. 4 Extreme d and θ^{-1} situations (ERA5). Composite maps of SLP anomalies in hPa (contours), density of jet positions (colors) and associated mean position (orange lines) for the days with extreme values of the local dimension d and the local persistence θ^{-1}. The black dashed lines are the main modes (more than 30% of the trajectories) and the gray dashed lines are the minor modes (less than 30% of the trajectories).

4 Interdecadal variations of the eddy-driven jet stream

Figure 6 panels (a) and (b) present the temporal evolution of the one-year rolling mean of the d and θ^{-1} indicators computed on the jet position vectors for the ERA20C reanalysis data set over the 1900-2010 period. A Gaussian filter with a cut-off frequency of 5 years was applied on the raw time series for obtaining the smoothed time series. The 5 years cut-off frequency was chosen to average out most inter-annual variability (e.g. ENSO). Both indicators display substantial inter-annual variability, up to ∼30% (6.5 to 8.5) with respect to its mean for local dimension but only ∼10% with respect to its mean for local persistence (3.5 to 3.8). When computing the wavelet spectrum on the raw time series of our indicators (panel (c)) one sees a strong peak at the one year period, which corresponds to the annual cycle. For higher periods, the log-log plot shows that the indicators behave as red noises (straight line), except around the 50 years period where a dominant peak emerges. We ran a similar spectrum analysis over the 1950-2020 period for the ERA5 data set and found a similar peak around the 50 years period (Fig. 11). This peak is also seen when using other indicators (Fig. 5). Nonetheless, a 50 year period in a 110 (or 70) years data set is near the limit of detectability, therefore we cannot assert that this is a relevant feature of the jet variability.

Fig. 6 panel (a) displays a decrease of local dimension from 1970 to 1990 and then an increase up to 2000. This interdecadal variation is large even after applying a 5-year low pass filter (∼10% of the mean value). A well documented phenomenon occurred in the North Atlantic ocean during the period 1970-2000 (Sutton and Dong, 2012; Robson et al, 2016; Jackson et al, 2022). The European climate experienced substantial changes, with anomalously mild, wet, summers in Northern Europe, and hot, dry, summers in Southern Europe. This coincided with a major warming of the North Atlantic Ocean due to a

strengthening of the Atlantic Meridional Overturning Circulation (AMOC). On Fig. 11 we also see an increase of inter-decadal variability between the periods 1950-1980 and 1990-2020. Using a Levene's test (Levene, 1961) to compare the difference in variance between the two periods, we find significantly different ($p < 0.001$) standard deviations between the one-year rolling mean value of d distributions of the two periods: 0.25 for the 1950-1980 period and 0.33 for the 1990-2020 period.

Figure 5 shows the same plot for the $\bar{U}$, $\bar{Y}$ and W indicators. The mean speed and position indicators show no peculiar evolution during the 1970-2000 period. The W indicator however seems to display a similar evolution. It should be noted that these changes in the observed behavior of the North-Atlantic eddy-driven jet stream between the 1950-1980 and 1990-2010/2020 periods may be due to different data collection processes. It is indeed well-known that the so-called satellite era beginning in the 1980s increased by a large factor the quantity of available data. The large scale structures of the atmosphere are usually well resolved in reanalysis data (e.g. Slivinski et al (2021)), nonetheless we cannot completely rule out the possibility that the observed changes are not physically relevant features of the jet (see (Rodrigues et al, 2018) for a similar discussion). The purpose of this paper is not to evaluate whether these changes are artifacts of the data collection process, but one should be cautious when attributing these results to a real physical behavior of the jet position.

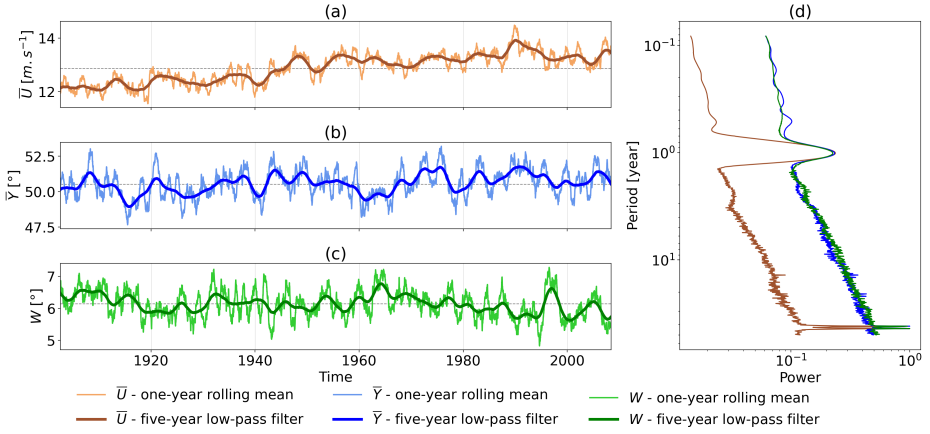

Fig. 5 Time series and power spectrum of $\bar{U}$, $\bar{Y}$ and W (ERA20C). (a) Time series of $\bar{U}$ with a one-year rolling mean and a five-year low-pass filter. (b) Time series of $\bar{Y}$ with a one-year rolling mean and a five-year low-pass filter. (c) Time series of W with a one-year rolling mean and a five-year low-pass filter. (d) Wavelet spectrum of $\bar{U}$, $\bar{Y}$ and W.

We now wish to estimate the effect of global warming on the variability of the jet using our dynamical indicators as a relevant measure of "variability". Isolating the contribution of global warming to the observed changes in the behavior of the jet is not straightforward in so far as the jet displays a large

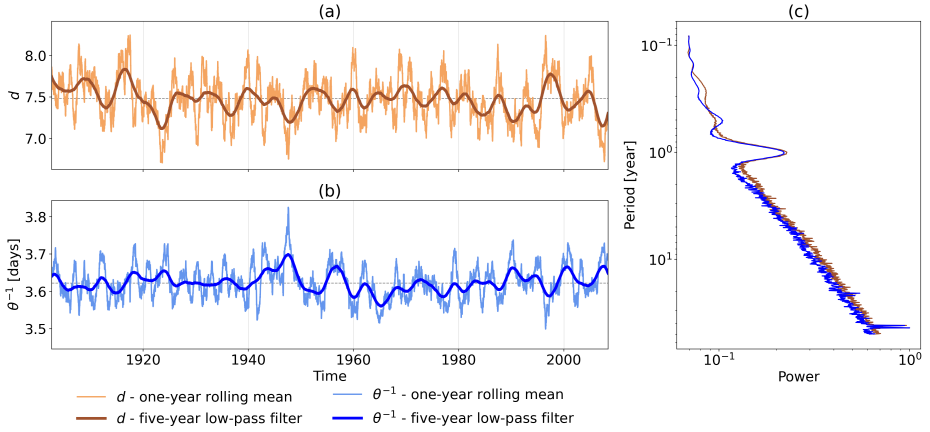

Fig. 6 Time series and power spectrum of d and θ^{-1} (ERA20C). (a) Time series of d with a one-year rolling mean and a five-year low-pass filter. (b) Time series of θ^{-1} with a one-year rolling mean and a five-year low-pass filter. (c) Wavelet spectrum of d and θ^{-1}.

variability and any signal of forced change may therefore be obscured by the influence of other factors. Controlling for these factors would allow to isolate the global warming signal, but one should take care of controlling only for the relevant factors. It is necessary to control only for factors that are confounders of the link between global warming and the variability of the jet (Kretschmer et al, 2021). Based on existing literature (Newman et al, 2016; Levine et al, 2017; Lin and Qian, 2022), we propose the causal graph depicted in figure 7. This graph summarizes our hypotheses for quantifying the impact of global warming on the jet variability on inter-decadal timescales.

Potential confounders of the variability of the North-Atlantic eddy-driven jet stream and global warming are supposed to be the AMO, the ENSO, the PDO and Aerosols Radiative Forcing (ARF). The variability of the jet is strongly linked to anomalies of SSTs in the North Atlantic (Simpson et al, 2018), therefore it is natural to posit an impact of the AMO on the jet, even though here we do not precise what is the exact physical phenomenon by which the AMO influences the jet. The impact of the ENSO and the PDO on the Euro-Atlantic climate are also well documented (Ding et al, 2017; Mezzina et al, 2020), and these two modes influence the inter-decadal variability of the global temperature of the Earth (Foster and Rahmstorf, 2011). To the natural variability of the ocean presented by the AMO, the ENSO and the PDO, we add the ARF over the Euro-Atlantic sector in so far as the changes in the emissions of aerosols can alter the global circulation (Pausata et al, 2015; Diao and Xu, 2022; Murakami, 2022). To measure this quantity, we average over the Euro-Atlantic sector the aerosols optical thickness at 550nm computed using the IPSL-CM5 model (Dufresne et al, 2013) which uses the same forcing files as the ERA20C and ERA5 reanalysis. As documented by Qin et al (2020),

ARF impacted the AMO over the 20th century, but this mode still has its one variability.

One may note that the causal model we are estimating does not show any feedback loop between global warming and the AMO, the PDO and the ENSO. The SSTs of the oceanic regions on which those indicators are computed did change during the 20th century in response to the radiative forcing caused by anthropogenic emissions, but here we use the detrended time series of these indicators. We therefore explicitly assume that the global increase of temperature on the Earth had no impacts on the natural evolution of the AMO, PDO and ENSO indicators over the period studied that is not taken into account when removing a linear trend (Trenberth and Shea, 2006). For small increases of the global temperature, this hypothesis is reasonable. However, when extrapolating our results in the future with a much larger warming level, this hypothesis may prove to be wrong.

We use monthly-averaged normalized time series and we apply low-pass Gaussian filters with 2, 5 and 10-year cut-off frequencies to ensure robustness with respect to the time-filtering procedure. The rationale for using low-pass filters with cut-off frequencies greater than 2 years is to remove any variations that are irrelevant at the inter-decadal time scale, the main one being the annual cycle. For the filters with 5 and 10-year cut-off frequencies, it may be possible that the ENSO signal is filtered out and therefore we will mainly interpret the results found using the 2-year filter. For simplicity reasons, we choose to estimate a linear model. The model is the following:

$$\text{Jet} = \alpha \text{T} + \beta \text{AMO} + \delta \text{PDO} + \gamma \text{ENSO} + \nu \text{ARF} + \epsilon. \quad (1)$$

In equation 1, the "Jet" variable represents the different indicators on which we compute the regression. The ϵ term represents a random noise. Even though controlling for the AMO, the PDO, the ENSO and the ARF is essential to estimate the causal effect of T, we stress that their associated coefficients cannot be interpreted as a total causal effect of their respective phenomena on the variability of the jet. We are estimating only a limited part of the causal graph, therefore we only interpret the α coefficient associated with the T parameter.

Figure 8 displays the results of the estimation of the α coefficient in equation 1 for the local dimension d, the local persistence θ^{-1}, the mean speed of the jet $\bar{U}$, the mean position of the jet $\bar{Y}$, the waviness of the jet W, the jet latitude index JLI and the zonal wind speed at the jet latitude index U_{JLI} using the ERA20C data set over the period 1900-2010. All estimated coefficients are significant at the 5% level when estimating 95% confidence intervals with a maximum likelihood estimator. Results are stable when applying different cut-off frequencies for the low-pass filter. We found that global warming significantly decreases the local dimension d and the waviness W of the jet position. We also found that global warming increases the mean speed $\bar{U}$ and the zonal wind speed U_{JLI} at the JLI. Finally, global warming causes a poleward shift of the position of the eddy-driven jet, measured using either the

mean position $\bar{Y}$ or the JLI. When going back to dimensionalized units, we estimate that a 1K increase of the global temperature of the Earth leads to a decrease of 2.3% [1.8,2.9] of the local dimension and 7.0% [5.9,8.0] of the waviness of the jet position with respect to their mean over the 1900-2010 period. It also leads to an increase of the local persistence by 0.4% [0.2,0.5], of the mean speed by 10.5% [10.1,10.9], of the zonal wind speed at the JLI by 11.3% [10.5,12.1], of the mean position by 1.5% [1.2,1.8] and of the JLI by 1.8% [1.3,2.3].

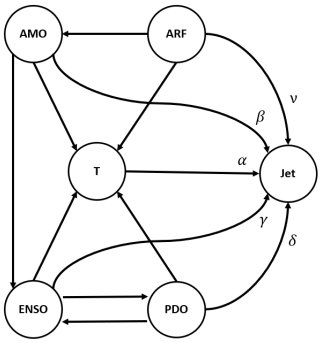

Fig. 7 Estimated causal graph of the influence of global warming on the jet. AMO stands for Atlantic Meridional Oscillation, ENSO for El-Nino Southern Oscillation, PDO for Pacific Decadal Oscillation, ARF for Aerosols Radiative Forcing and T for global mean temperature of the Earth.

Figure 12 in annex presents the same analysis using the ERA5 data set over the 1950-2020 period. Broadly speaking, the estimations of the α coefficient are much less precise and many coefficients are not statistically different from zero. The decrease of waviness is still significant when using the 2-year and 5-year filters, but this is not the case for local dimension. The result on local persistence depends on the filter considered and are overall close to zero. For jet speed, the mean speed $\bar{U}$ does not seem to be affected by global warming and the results point towards different directions for U_{JLI}. The northward shift of the mean position of the jet is better estimated, using either $\bar{Y}$ or JLI, but the significance of the evolution depends on the filter cut-off frequency.

5 Discussion and conclusions

We studied the variability of the North Atlantic eddy-driven jet stream described by its instantaneous latitudinal position at each longitude. We used indicators from dynamical system theory to characterize the underlying attractor on which the jet is evolving. We showed using that this representation is more relevant to characterize the jet variability than using the more classical Z500 and SLP fields and associated weather regimes. Z500 and SLP fields

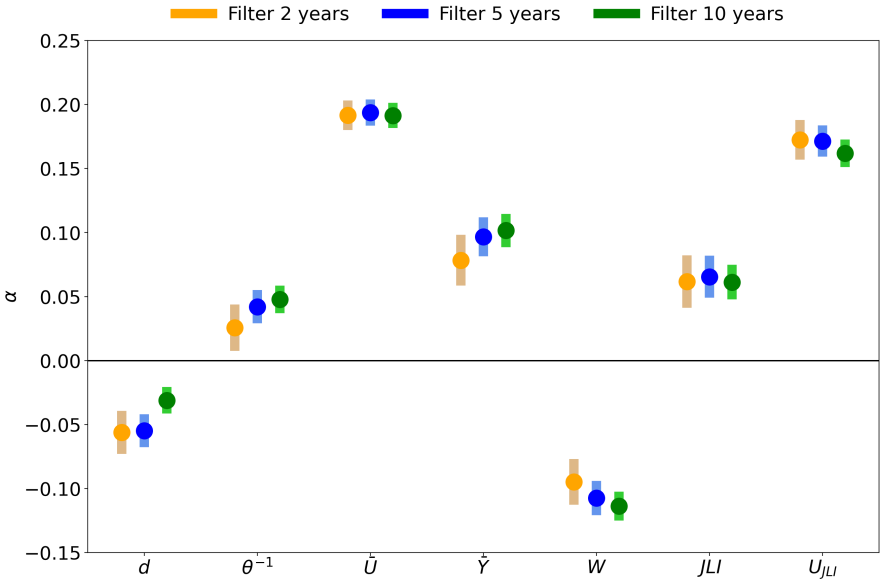

Fig. 8 Estimation of the impact of global warming on indicators of the jet variability (ERA20C). The plot represents the estimated α coefficient for the local dimension d, the local persistence θ^{-1}, the mean speed of the jet $\bar{U}$, the mean position of the jet $\bar{Y}$, the waviness of the jet W, the jet latitude index JLI and the zonal wind speed at the jet latitude index U_{JLI}. The dots represent the estimated coefficient and the shaded vertical bars the associated 95% confidence interval. The orange (resp. blue and green) estimation is found using the time series after applying a 2-year (resp. 5-year and 10-year) low-pass Gaussian filter. All time series are monthly averages.

carry more information than needed and targeting the jet position per se as we did allows to focus on the sole dynamics of the jet.

We then studied the inter-decadal variability of the jet using the dynamical indicators. After controlling for potential confounders between the global temperature of the Earth and the jet, we are able to quantify the impact of global warming on key indicators of the jet behavior. We showed that, over the 1900-2010 period, global warming decreased the local dimension and waviness of the jet position and increased its local persistence. Global warming also increased the wind speed of the jet and shifted its mean position to the north. The decrease of waviness and poleward shift results hold using the ERA5 data set over the period 1950-2020, but this is not the case for the other indicators.

Faranda et al (2019a) and Rodrigues et al (2018) also showed a decrease in local dimension over the North-Atlantic for the SLP field in future warming scenarios. Faranda et al (2019a) attribute this decrease to the warming of the ocean. Our results suggest a similar mechanism may apply to the eddy-driven jet. The poleward shift, strengthening and zonalisation of the Euro-Atlantic eddy-driven jet stream scenario that we found here is coherent with the recent work of Blackport and Screen (2020) who found similar results using different metrics on the mid- and upper-troposphere mid-latitudes circulation. We do

find an increase in the variability of the jet over the 1990-2020 period with respect to the 1950-1980 period. However, our regression analysis suggests the recent positive phase of the AMO partially offset the decrease in variability of the eddy-driven jet, leading to this paradoxical observation. This would explain the contradicting results found in the literature on the recent changes of the variability of the jet stream (Francis and Vavrus, 2015; Coumou et al, 2015; Harvey et al, 2020).

The validity of the results we showed depends crucially on the capacity of the reanalysis data sets to reproduce correctly the behavior of the North-Atlantic eddy-driven jet stream in the past. Even though the large structures of the atmosphere are probably the features best resolved by reanalysis (Slivinski et al, 2021), there is no doubt that the reanalysis over the period 1980-2020, the so-called satellite era, provide much better results than in the previous periods. It is not clear whether we should have more confidence on the results found on the ERA5 data set over the period 1950-2020 or on the ERA20C data set over the period 1900-2010. The properties of the jet are probably closer to reality in the first data set but the natural variability of the climate system is better sampled in the second. Therefore, even though we used a causal inference framework to disentangle the influence of confounders from the influence of global warming of the Earth on the jet, we cannot assert that our results give the causal impact of global warming on the variability of the jet.

Finally, our results demonstrate the interest of using tools from dynamical system theory to target specific patterns of the large scale atmospheric circulation and quantify their natural and forced variability. We also think that these tools could be used to evaluate whether climate models are able to represent correctly the natural variability of the jet position and we are currently investigating this question.

Acknowledgments. The authors wish to thank S Charbit, P Yiou, G Messori, T Caby, A Hisi and B Colnet for their fruitful inputs.

Declarations

- Funding: This work has received support from the European Union's Horizon 2020 research and innovation programme under grant agreement No. 101003469 (XAIDA), by the European Research Council (ERC) under by the Marie Sklodowska-Curie grant agreement No. 956396 (EDIPI).
- Conflict of interest: The authors declare no conflict of interest.
- Ethics approval: Not applicable.
- Consent to participate: Not applicable.
- Consent for publication: Not applicable.
- Availability of data and materials: The ERA5 and ERA20C are available on the Copernicus web site (https://cds.climate.copernicus.eu/). The results of the detection procedure and the time series of indicators are available on demand.

- Code availability: The main results of this work were obtained using Python. The scripts are available upon request.
- Authors' contributions: RN designed the analysis. Material preparation, data collection and analysis were performed by VG, AV and RN. All authors contributed to the writing of the paper.

Appendix

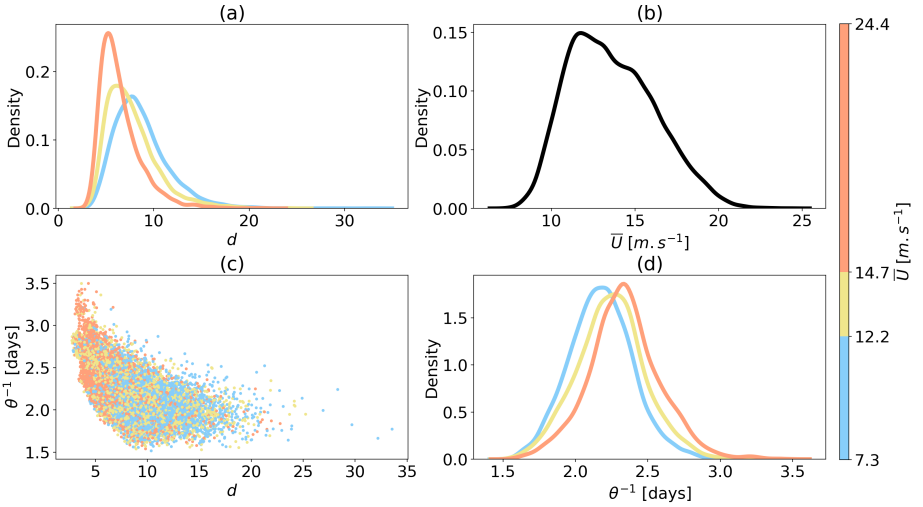

Fig. 9 Link between the dynamical indicators and the jet mean speed. (a) Distribution of local dimension d for the three terciles of the mean speed $\bar{U}$. (b) Distribution of $\bar{U}$. (c) Cross distribution of d and θ^{-1} colored by the tercile of the $\bar{U}$ indicator. (d) Distribution of local persistence θ^{-1} for the three terciles of the mean speed $\bar{U}$.

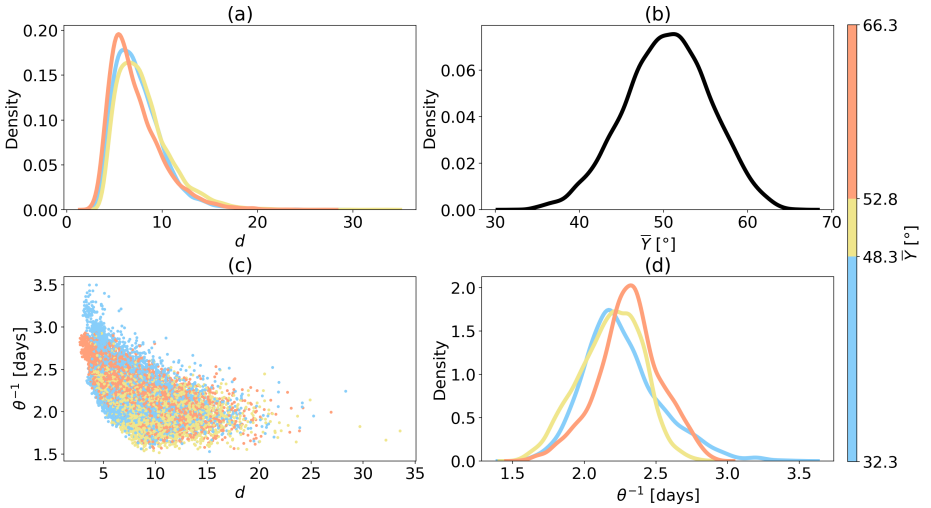

Fig. 10 Link between the dynamical indicators and the jet mean position. (a) Distribution of local dimension d for the three terciles of the mean position $\bar{Y}$. (b) Distribution of $\bar{Y}$. (c) Cross distribution of d and θ^{-1} colored by the tercile of the $\bar{Y}$ indicator. (d) Distribution of local persistence θ^{-1} for the three terciles of the mean position $\bar{Y}$.

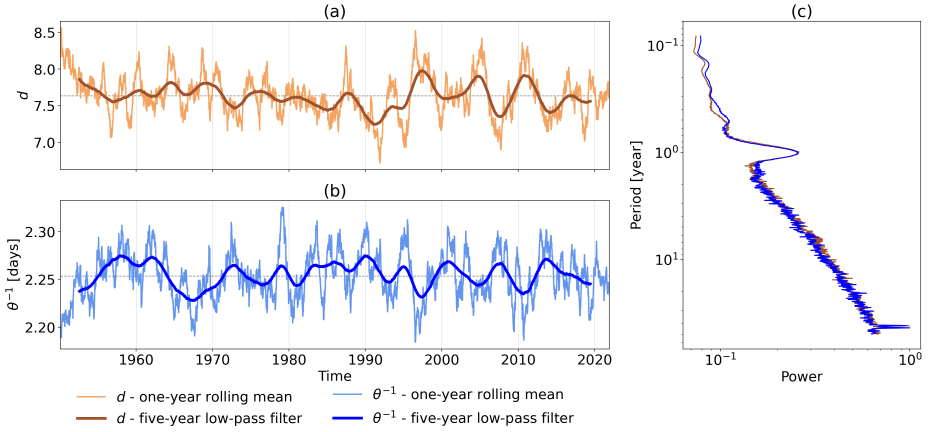

Fig. 11 Time series and power spectrum of d and θ^{-1} (ERA5). (a) Time series of d with a one-year rolling mean and a five-year low-pass filter. (b) Time series of θ^{-1} with a one-year rolling mean and a five-year low-pass filter. (c) Wavelet spectrum of d and θ^{-1}.

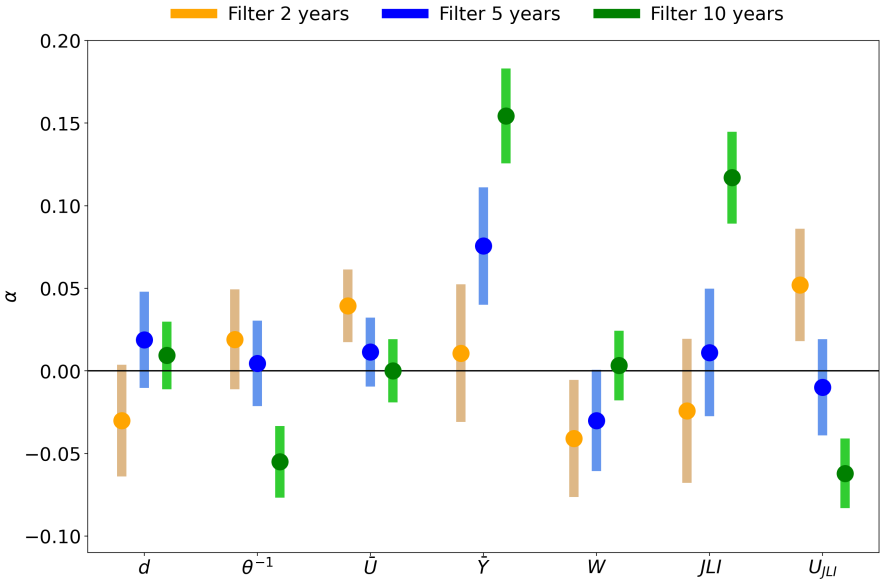

Fig. 12 Estimation of the impact of global warming on indicators of the jet variability (ERA5). The plot represents the estimated α coefficient for the local dimension d, the local persistence θ^{-1}, the mean speed of the jet $\bar{U}$, the mean position of the jet $\bar{Y}$, the waviness of the jet W, the jet latitude index JLI and the zonal wind speed at the jet latitude index U_{JLI}. The dots represent the estimated coefficient and the shaded vertical bars the associated 95% confidence interval. The orange (resp. blue and green) estimation is found using the time series after applying a 2-year (resp. 5-year and 10-year) low-pass Gaussian filter. All time series are monthly averages.

References

Barnes EA, Screen JA (2015) The impact of arctic warming on the midlatitude jet-stream: Can it? has it? will it? Wiley Interdisciplinary Reviews: Climate Change 6(3):277–286

Blackport R, Screen JA (2020) Insignificant effect of arctic amplification on the amplitude of midlatitude atmospheric waves. Science advances 6(8):eaay2880

Cattiaux J, Peings Y, Saint-Martin D, et al (2016) Sinuosity of midlatitude atmospheric flow in a warming world. Geophysical Research Letters 43(15):8259–8268

Charney J (1947) The dynamics of long waves in a baroclinic. Westerly Current, J Meteorol 4

Cohen J, Zhang X, Francis J, et al (2018) Arctic change and possible influence on mid-latitude climate and weather: a us clivar white paper. US CLIVAR reports

Coumou D, Lehmann J, Beckmann J (2015) The weakening summer circulation in the northern hemisphere mid-latitudes. Science 348(6232):324–327

Diao C, Xu Y (2022) Reassessing the relative role of anthropogenic aerosols and natural decadal variability in driving the mid-twentieth century global "cooling": a focus on the latitudinal gradient of tropospheric temperature. Climate Dynamics pp 1–27

Ding S, Chen W, Feng J, et al (2017) Combined impacts of pdo and two types of la niña on climate anomalies in europe. Journal of climate 30(9):3253–3278

Dorrington J, Strommen K (2020) Jet speed variability obscures euro-atlantic regime structure. Geophysical Research Letters 47(15):e2020GL087,907

Duchon CE (1979) Lanczos filtering in one and two dimensions. Journal of Applied Meteorology and Climatology 18(8):1016–1022

Dufresne JL, Foujols MA, Denvil S, et al (2013) Climate change projections using the ipsl-cm5 earth system model: from cmip3 to cmip5. Climate dynamics 40(9):2123–2165

Faranda D, Messori G, Yiou P (2017) Dynamical proxies of north atlantic predictability and extremes. Scientific reports 7(1):1–10

Faranda D, Alvarez-Castro MC, Messori G, et al (2019a) The hammam effect or how a warm ocean enhances large scale atmospheric predictability. Nature Communications 10:1316

Faranda D, Sato Y, Messori G, et al (2019b) Minimal dynamical systems model of the northern hemisphere jet stream via embedding of climate data. Earth System Dynamics 10(3):555–567

Foster G, Rahmstorf S (2011) Global temperature evolution 1979–2010. Environmental research letters 6(4):044,022

Francis JA, Vavrus SJ (2015) Evidence for a wavier jet stream in response to rapid arctic warming. Environmental Research Letters 10(1):014,005

Hallam S, Josey SA, McCarthy GD, et al (2022) A regional (land–ocean) comparison of the seasonal to decadal variability of the northern hemisphere jet stream 1871–2011. Climate Dynamics pp 1–22

Harvey B, Cook P, Shaffrey L, et al (2020) The response of the northern hemisphere storm tracks and jet streams to climate change in the cmip3, cmip5, and cmip6 climate models. Journal of Geophysical Research: Atmospheres 125(23):e2020JD032,701

Held IM (1975) Momentum transport by quasi-geostrophic eddies. J Atmos Sci 32(7):1494–1497

Held IM (1993) Large-scale dynamics and global warming. Bulletin of the American Meteorological Society 74(2):228–242

Held IM, Hou AY (1980) Nonlinear axially symmetric circulations in a nearly inviscid atmosphere. Journal of the Atmospheric Sciences 37(3):515–533

Hersbach H, Bell B, Berrisford P, et al (2020) The era5 global reanalysis. Quarterly Journal of the Royal Meteorological Society 146(730):1999–2049

Hochman A, Alpert P, Harpaz T, et al (2019) A new dynamical systems perspective on atmospheric predictability: Eastern mediterranean weather regimes as a case study. Science advances 5(6):eaau0936

Holton JR (1973) An introduction to dynamic meteorology. American Journal of Physics 41(5):752–754

Hoskins BJ, James IN (2014) Fluid dynamics of the mid-latitude atmosphere. John Wiley & Sons

Hurrell JW, Deser C (2010) North atlantic climate variability: the role of the north atlantic oscillation. Journal of marine systems 79(3-4):231–244

Iqbal W, Leung WN, Hannachi A (2018) Analysis of the variability of the north atlantic eddy-driven jet stream in cmip5. Climate Dynamics 51(1):235–247

Jackson LC, Biastoch A, Buckley MW, et al (2022) The evolution of the North Atlantic Meridional Overturning Circulation since 1980. Nature Reviews Earth & Environment 3:241–254

Kautz LA, Martius O, Pfahl S, et al (2022) Atmospheric blocking and weather extremes over the euro-atlantic sector–a review. Weather and Climate Dynamics 3(1):305–336

Kerr RA (2000) A north atlantic climate pacemaker for the centuries. Science 288(5473):1984–1985

Kretschmer M, Adams SV, Arribas A, et al (2021) Quantifying causal pathways of teleconnections. Bulletin of the American Meteorological Society 102(12):E2247–E2263

Lee JY, Marotzke J, Bala G, et al (2021) Future Global Climate: Scenario-Based Projections and Near-Term Information. In Climate Change 2021: The Physical Science Basis. Contribution of Working Group I to the Sixth Assessment Report of the Intergovernmental Panel on Climate Change. Cambridge University Press

Lee S, Kim Hk (2003) The dynamical relationship between subtropical and eddy-driven jets. Journal of the atmospheric sciences 60(12):1490–1503

Levene H (1961) Robust tests for equality of variances. Contributions to probability and statistics Essays in honor of Harold Hotelling pp 279–292

Levine AF, McPhaden MJ, Frierson DM (2017) The impact of the amo on multidecadal enso variability. Geophysical Research Letters 44(8):3877–3886

Limbach S, Schömer E, Wernli H (2012) Detection, tracking and event localization of jet stream features in 4-d atmospheric data. Geoscientific Model Development 5(2):457–470

Lin J, Qian T (2022) The atlantic multi-decadal oscillation. Atmosphere-Ocean 60(3-4):307–337

Lucarini V, Faranda D, de Freitas JMM, et al (2016) Extremes and recurrence in dynamical systems. John Wiley & Sons

Messori G, Caballero R, Faranda D (2017) A dynamical systems approach to studying midlatitude weather extremes. Geophysical Research Letters 44(7):3346–3354

Messori G, Harnik N, Madonna E, et al (2021) A dynamical systems characterization of atmospheric jet regimes. Earth System Dynamics 12(1):233–251

682 Mezzina B, García-Serrano J, Bladé I, et al (2020) Dynamics of the enso tele-
683 connection and nao variability in the north atlantic–european late winter.
684 Journal of Climate 33(3):907–923

685 Michelangeli PA, Vautard R, Legras B (1995) Weather regimes: Recurrence
686 and quasi stationarity. Journal of the atmospheric sciences 52(8):1237–1256

687 Mitchell D, Kornhuber K, Huntingford C, et al (2019) The day the 2003
688 european heatwave record was broken. The Lancet Planetary Health
689 3(7):e290–e292

690 Molnos S, Mamdouh T, Petri S, et al (2017) A network-based detection scheme
691 for the jet stream core. Earth System Dynamics 8(1):75–89

692 Moloney NR, Faranda D, Sato Y (2019) An overview of the extremal index.
693 Chaos: An Interdisciplinary Journal of Nonlinear Science 29(2):022,101

694 Moon W, Kim BM, Yang GH, et al (2022) Wavier jet streams driven by zonally
695 asymmetric surface thermal forcing. Proceedings of the National Academy
696 of Sciences 119(38):e2200890,119

697 Morice CP, Kennedy JJ, Rayner NA, et al (2021) An updated assessment of
698 near-surface temperature change from 1850: the hadcrut5 data set. Journal
699 of Geophysical Research: Atmospheres 126(3):e2019JD032,361

700 Murakami H (2022) Substantial global influence of anthropogenic aerosols on
701 tropical cyclones over the past 40 years. Science advances 8(19):eabn9493

702 Newman M, Alexander MA, Ault TR, et al (2016) The pacific decadal
703 oscillation, revisited. Journal of Climate 29(12):4399–4427

704 van Oldenborgh GJ, te Raa LA, Dijkstra HA, et al (2009) Frequency-or
705 amplitude-dependent effects of the atlantic meridional overturning on the
706 tropical pacific ocean. Ocean science 5(3):293–301

707 Osman MB, Coats S, Das SB, et al (2021) North atlantic jet stream projections
708 in the context of the past 1,250 years. Proceedings of the National Academy
709 of Sciences 118(38)

710 Pausata FSR, Gaetani M, Messori G, et al (2015) The role of aerosol in altering
711 north atlantic atmospheric circulation in winter and its impact on air quality.
712 Atmospheric Chemistry and Physics 15(4):1725–1743

713 Peings Y, Cattiaux J, Vavrus SJ, et al (2018) Projected squeezing of the
714 wintertime north-atlantic jet. Environmental Research Letters 13(7):074,016

715 Pena-Ortiz C, Gallego D, Ribera P, et al (2013) Observed trends in the global
716 jet stream characteristics during the second half of the 20th century. Journal

of Geophysical Research: Atmospheres 118(7):2702–2713

Pickands J (1975) Statistical inference using extreme order statistics. The Annals of Statistics 3(1):119–131. URL http://www.jstor.org/stable/2958083

Poli P, Hersbach H, Dee DP, et al (2016) Era-20c: An atmospheric reanalysis of the twentieth century. Journal of Climate 29(11):4083–4097

Pons FME, Messori G, Alvarez-Castro MC, et al (2020) Sampling hyperspheres via extreme value theory: implications for measuring attractor dimensions. Journal of statistical physics 179(5):1698–1717

Qin M, Dai A, Hua W (2020) Quantifying contributions of internal variability and external forcing to atlantic multidecadal variability since 1870. Geophysical Research Letters 47(22):e2020GL089,504

Rhines PB (1975) Waves and turbulence on a beta-plane. Journal of Fluid Mechanics 69(3):417–443

Robson J, Ortega P, Sutton R (2016) A reversal of climatic trends in the north atlantic since 2005. Nature Geoscience 9

Rodrigues D, Alvarez-Castro MC, Messori G, et al (2018) Dynamical properties of the north atlantic atmospheric circulation in the past 150 years in cmip5 models and the 20crv2c reanalysis. Journal of Climate 31(15):6097–6111

Röthlisberger M, Pfahl S, Martius O (2016) Regional-scale jet waviness modulates the occurrence of midlatitude weather extremes. Geophysical Research Letters 43(20):10–989

Simpson IR, Deser C, McKinnon KA, et al (2018) Modeled and observed multidecadal variability in the north atlantic jet stream and its connection to sea surface temperatures. Journal of Climate 31(20):8313–8338

Simpson IR, Yeager SG, McKinnon KA, et al (2019) Decadal predictability of late winter precipitation in western Europe through an ocean-jet stream connection. Nature Geoscience 12(8):613–619

Slivinski L, Compo G, Sardeshmukh P, et al (2021) An evaluation of the performance of the twentieth century reanalysis version 3. Journal of Climate 34(4):1417–1438

Spensberger C, Spengler T (2020) Feature-based jet variability in the upper troposphere. Journal of Climate 33(16):6849–6871

Spensberger C, Spengler T, Li C (2017) Upper-tropospheric jet axis detection and application to the boreal winter 2013/14. Monthly Weather Review 145(6):2363–2374

Stendel M, Francis J, White R, et al (2021) The jet stream and climate change. In: Climate Change. Elsevier, p 327–357

Sutton R, Dong B (2012) Atlantic ocean influence on a shift in european climate in the 1990s. Nature Geoscience 5:788–792

Süveges M (2007) Likelihood estimation of the extremal index. Extremes 10(1):41–55

Tenenbaum J, Williams PD, Turp D, et al (2022) Aircraft observations and reanalysis depictions of trends in the north atlantic winter jet stream wind speeds and turbulence. Quarterly Journal of the Royal Meteorological Society

Trenberth KE, Shea DJ (2006) Atlantic hurricanes and natural variability in 2005. Geophysical research letters 33(12)

Van Oldenborgh GJ, Hendon H, Stockdale T, et al (2021) Defining el niño indices in a warming climate. Environmental research letters 16(4):044,003

Woollings T, Hannachi A, Hoskins B (2010) Variability of the north atlantic eddy-driven jet stream. Quarterly Journal of the Royal Meteorological Society 136(649):856–868

Woollings T, Czuchnicki C, Franzke C (2014) Twentieth century north atlantic jet variability. Quarterly Journal of the Royal Meteorological Society 140(680):783–791

Woollings T, Barnes E, Hoskins B, et al (2018) Daily to decadal modulation of jet variability. Journal of Climate 31(4):1297–1314